17th World Conference on Earthquake Engineering, 17WCEE
Sendai, Japan - September 13th to 18th 2020

MASS TIMBER BUCKLING-RESTRAINED BRACE FOR SEISMIC REGIONS

C.P. Pantelides[(1)], C. Murphy[(2)], H.E. Blomgren[(3)], D.R. Rammer[(4)]

[(1)] *Professor, Dept. Civil and Environmental Engineering, University of Utah, Salt Lake City, UT, USA, c.pantelides@utah.edu*
[(2)] *Res. Asst., Dept. Civil and Environmental Engineering, University of Utah, Salt Lake City, UT, USA, coltonfmurphy@gmail.com*
[(3)] *Director of Testing and Characterization, Katerra, Seattle, WA, USA, hans-erik.blomgren@katerra.com*
[(4)] *Research General Engineer, Forest Products Laboratory, Madison, WI, USA, douglas.r.rammer@usda.gov*

Abstract

Multi-story commercial mass timber buildings are sustainable since wood is renewable and stores carbon dioxide in the wood mass. However, conventional timber braced frame lateral force resisting systems lack the satisfactory ductility and hysteretic energy dissipation necessary in seismic regions. A mass timber braced frame (T-BRBF) using a mass timber buckling-restrained brace (T-BRB) is proposed to provide the necessary hysteretic energy dissipation and reduce seismic demands. Design and testing of the T-BRB is described which combines the ductility of a yielding steel core with the elastic confinement provided by a mass timber casing. Compression tests of block specimens were carried out to investigate candidate materials for constructing the T-BRB casing including glued laminated timber (Glulam), laminated veneer lumber (LVL), parallel strand lumber (PSL), and mass plywood panel (MPP). The objective of the compression tests was to evaluate the load versus deformation behavior of the specimens, when loaded in compression, with or without compression screw reinforcement. MPP loaded parallel to laminations exhibited the best performance characteristics because of the unique orthogonal layup of veneer laminations that provides high elastic stiffness and restrains the steel core short wave buckling failure mode. When MPP is loaded parallel to the wide face of the laminations, 50% of the veneers are orientated such that the stiff axes are aligned with the applied bearing load. Six 3.60 m-long T-BRBs with a 275 kN design yield strength were constructed and tested under quasi-static cyclic loading utilizing three different MPP casing grade layups. For each casing type, two quasi-static loading protocols were used: (a) low-cycle fatigue, and (b) high strain. The T-BRBs exhibited stable hysteretic behavior, superior hysteretic energy dissipation, and cumulative inelastic axial deformation well over 200 times the steel core yield deformation acceptance criteria prescribed in the AISC-341 Standard.

Keywords: buckling; brace; damper; steel; timber.

1. Introduction

Buckling-Restrained Braced Frames (BRBF) are a reliable method for providing an efficient lateral force resisting system for new and retrofitting of existing structures in earthquake prone regions. The Buckling-Restrained Brace (BRB) is a fuse-type element which facilitates stable energy dissipation and is replaceable after an earthquake. Heavy timber vertical structures are in need of a lightweight and economic timber lateral load resisting system that provides the benefits of a BRBF. The aim of this research is to develop a mass timer BRB that is easy to manufacture and feasible to implement by combining a steel core with a mass timber casing, the Timber-Buckling Restrained Brace (T-BRB). T-BRBs have advantages compared to their composite steel and concrete counterpart including recyclability, sustainability and performance. Moreover, they can easily be inspected after an earthquake to determine their condition and whether they should be replaced.

BRBs provide satisfactory stiffness, strength and stable energy dissipation [1]; in addition, they provide adequate rigidity to satisfy drift limits. Advancements in timber technology are making high rise mass timber buildings attractive. Mass timber buildings attract less inertial forces, however, they lack a code-defined lateral force resisting system [2]; a buckling restrained brace with a Glulam casing was built and tested under cyclic loads to determine its performance. The HT-BRB exhibited higher axial load, higher stiffness, more stable axial deformation capacity, and significantly greater energy dissipation characteristics when compared to conventional timber braces. Ductility, strength, stiffness and damping of conventional timber braces is a concern in high seismic regions and care must be taken in the design of the connections to reach high displacement ductility during an earthquake [3].

A buckling restrained brace concept using a lightweight casing made of wood has been presented [4]. Design of conventional BRB casing dimensions uses Euler buckling principles to avoid global buckling [5]. Research exploring the high-mode buckling response of conventional BRB steel cores has improved understanding of the internal modal response [6]. Methods to design the casing bolts were developed which resist both weak- and strong-axis steel core plate buckling forces common in conventional BRBs [7].

To optimize the T-BRB design, various types of timber block specimens were tested to determine mechanical properties that would be beneficial for a BRB casing. Wood type, screw reinforcement and direction of load, were considered as variables. Timber construction is establishing a reputation as sustainable and environmentally friendly. Timber is an excellent building material because it is renewable with a good strength to weight ratio, good insulating properties and acts as a means to store carbon dioxide. High rise timber structures will require an efficient and safe lateral force resisting system. Impressive high rise timber buildings of this nature, like the 18-story Mjøstårnet, a mass timber building recently completed in Norway, are being designed and constructed [8].

2. Engineered Timber Block Tests

The compressive tests conducted included both monotonic and cyclic tests. Fig. 1 shows the typical test setup using a hydraulic actuator. All mass timber specimens had a 152mm x 152mm x 305mm dimension. The following materials were tested: Mass Plywood Panel (MPP or M), Glulam (G), Parallel Strand Lumber (PSL or P), and Laminated Veneer Lumber (LVL or L). Glulam, MPP, and LVL specimens were loaded parallel and perpendicular to the wide face of the lamination/veneer while PSL specimens were only loaded perpendicular to the long axis of the wood strand. In addition, specimens were tested with and without compression screws used for reinforcement. Two repetitions of each type of test were carried out. A monotonic compression and quasi-static cyclic load protocol with a loading rate of 1 Hz were used until failure. Fig. 1(a) shows failure of an LVL specimen and Fig. 1(b) failure of a Glulam specimen without screw reinforcement. A sample of the load versus displacement behavior from the monotonic tests is shown in Fig. 2; the nomenclature is as follows: A=parallel to wide face of lamination/veneer (G, L, M) or parallel to long axis of wood strand (P); and U=unreinforced. Fig. 2 shows unreinforced specimens loaded monotonically parallel to the wide face of the lamination/veneer (G, L, M) or parallel to the long axis of the wood strand (P). Stiffness and maximum load are improved when compression is applied for MPP parallel to

the wide face of the laminations/veneers because 50% of the veneers are orientated such that the stiff axis is aligned with the applied load. Fig. 3 provides cyclic test results which show that MPP loaded perpendicular to the wide face of laminations has a lower yield force when compared to the case when it is loaded parallel to the wide face of laminations. In general, MPP loaded in the perpendicular orientation underperforms MPP loaded in the parallel orientation.

(a) (b)

Fig. 1 – Compression test setup: (a) LVL specimen at failure; (b) failure of unreinforced Glulam specimen

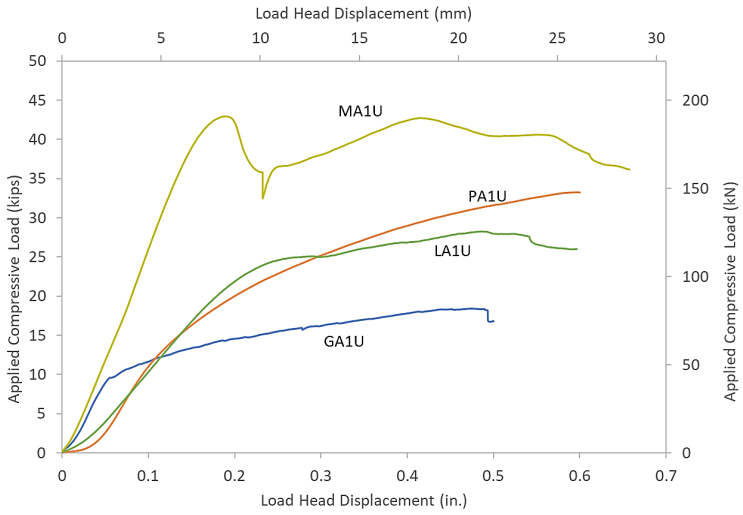

Fig. 2 – Results for unreinforced specimens monotonically loaded parallel to the wide face of the lamination/veneer (G, L, M) or parallel to the long axis of the wood strand (P)

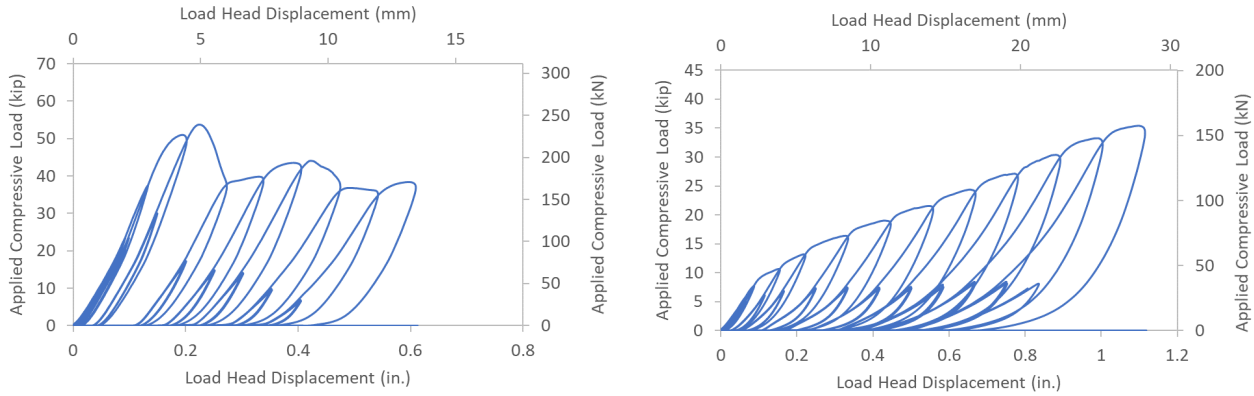

(a) (b)

Fig. 3 – Hysteresis curves for unreinforced MPP: (a) parallel to laminations; (b) perpendicular to laminations

Past research in timber buckling restrained braces has determined that a high elastic stiffness with a high compressive load is desirable for a T-BRB casing [2]. If the modulus of elasticity of the timber casing is too low, localized weak axis buckling occurs which leads to premature failure. Higher elastic stiffness in the timber casing promotes a consistent high mode weak axis buckling wavelength throughout the length of the core, which is desirable. Due to the manufacturing process, Glulam, LVL, and PSL have two distinctive orientations that are consistent with the underlying parallel and perpendicular to grain directions of wood. Unreinforced MPP loaded parallel to laminations outperformed Glulam, LVL and PSL and was adopted in this research for constructing the T-BRB casing.

3. T-BRB Element Tests

T-BRBs are capable of providing resistance in both compression and tension unlike conventional timber braces. T-BRBs act as a structural fuse element; they dissipate energy by yielding of the steel core therefore protecting the gravity load bearing system of a structure during a seismic event. T-BRBs can be replaced after being damaged and, unlike currently used steel BRBs, it is possible to inspect their steel core after an earthquake. Six 3.66 m long T-BRBs with a yield strength of 275 kN were tested in this research. Three T-BRBs were tested using a fatigue-based load protocol in which a high number of cycles was applied at a 1.5% strain, and the remaining T-BRBs were tested using a drift-based load protocol in which cycles of increasing strain were applied until failure.

3.1 T-BRB specimens

The six T-BRBs were constructed using 283 MPa steel cores and MPP casings as shown in Fig. 4. The steel core cross-section of the 2.49 m yielding length was 76 mm wide and 12.7 mm thick. The MPP casing was composed of two pieces that were 254 mm wide and 152 mm thick. Fig. 5 shows a 3D representation of the T-BRB. Stiffener plates were fabricated with the same steel as the steel core. The design value for yield strength was taken as 283 MPa and the tensile strength was taken as 431 MPa based on steel coupon tensile tests. The stiffener plates were welded to the core to prevent buckling outside of the timber casing. Two cheek plates were also welded to the ends of the T-BRBs around the pin connection to prevent a tearout failure. A steel dowel was welded to the core at its center to encourage an even distribution of core buckling forces. A hardwood spacer was used to provide bearing restraint against strong axis buckling of the core. A laminated beech wood material was used for the spacer. An offset was included in the design to allow for axial compression movement of the core.

Several 12.7 mm diameter, A449 bolts were used to connect the two sides of the MPP casing; these bolts were also used to fasten the hardwood spacer. A 178 mm spacing of the bolts was used throughout the yielding length of the BRB; however, this spacing was reduced near the ends of the BRB to account for an increase in out-of-plane forces that were predicted. Using Fig. 5(a) as the free body diagram of the buckled core inside the casing gives:

$$\Delta_{gap} = \nu \, \varepsilon_{max} \, t_f \tag{1}$$

where the original steel core thickness, t_f, is equal to 12.7 mm. Once the steel core goes into tension, a gap forms between the steel core and timber casing of increasing magnitude throughout the cyclic test due to Poisson effects. A Poisson's ratio, ν, of 0.5 was used for the steel core, which would be subjected to high strains and would be in the plastic region. This gap is equal to Δ_{gap} in Eq. (1); ε_{max} is the maximum tensile steel strain during the test and was assumed as 4.0%. By summing the moments in the free body diagram of Figs. 5(b), 5(c) and solving for P_b, the buckling force of the steel core, Eq. (2) is formed:

$$P_b = (4 \, P_{max} \, \nu \, \varepsilon_{max} \, t_f) \, / \, l_w \tag{2}$$

The wavelength of the buckled steel core, l_w, was assumed to be 11 times the thickness of the steel core or 140 mm [6]. P_{max} is the estimated maximum compressive force developed by the T-BRB; this value was estimated at 1.6 times the yield strength of the steel core to account for hardening and friction and a value of 445 kN was used. From Eq. (2), P_b is obtained as 3.2 kN, and this value was increased to 4.5 kN to

apply a safety factor of 1.4. This force was exerted onto the core throughout the yield length a total of 36 times due to the 140 mm wavelength spacing. This results in a total casing outward force of approximately 160 kN. By allocating 6.7 kN of allowable force per bolt, which considers bolt prestressing strength loss during the pneumatic torque tightening process, approximately (24) A449 bolts of 12.7 mm diameter were needed throughout the yield length of the core. The 178 mm bolt spacing provides 28 bolts throughout the 2.49 m yield zone. This spacing is a conservative estimate to avoid failure involving bolt fracture.

Three variations of MPP panels were used in the six T-BRB tests. Each 254 mm thick MPP plywood layout utilized a varying elastic modulus of 6896 MPa or 15168 MPa layers. The three MPP casing types were classified as soft, medium, and hard. Fig. 6 represents the layer layout for the three MPP specimen types. The soft specimens consisted of four center 25.4 mm thick layers of 6896 MPa plywood with three outer layers on each side of 15168 MPa plywood in Fig. 6(a). The medium specimens contained only two 25.4 mm wide layers of 6896 MPa with the remaining layers made of 15168 MPa plywood in Fig. 6(b). The hard specimens were entirely made of 15168 MPa layers in Fig. 6(c). Specimens 1-3 were soft, medium, and hard, respectively; specimens 4-6 were hard, medium, and soft, respectively.

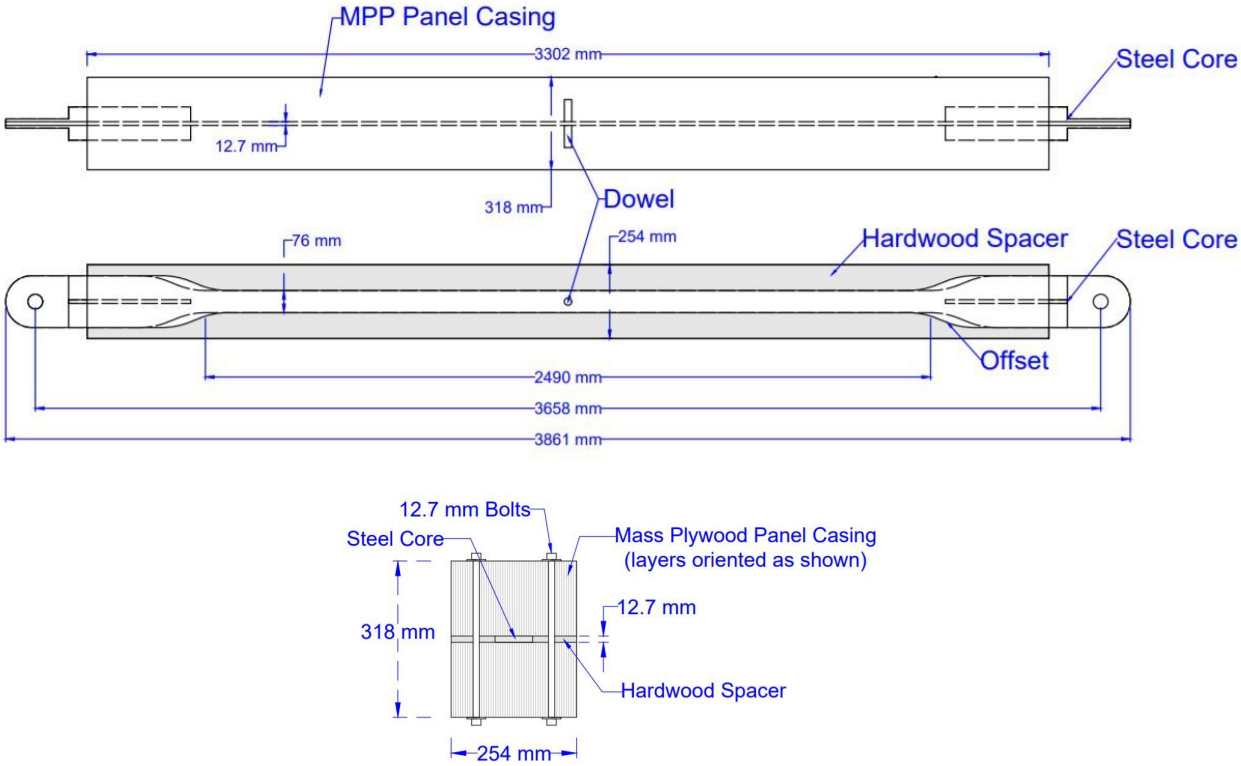

Fig. 4 – Timber-BRB layout

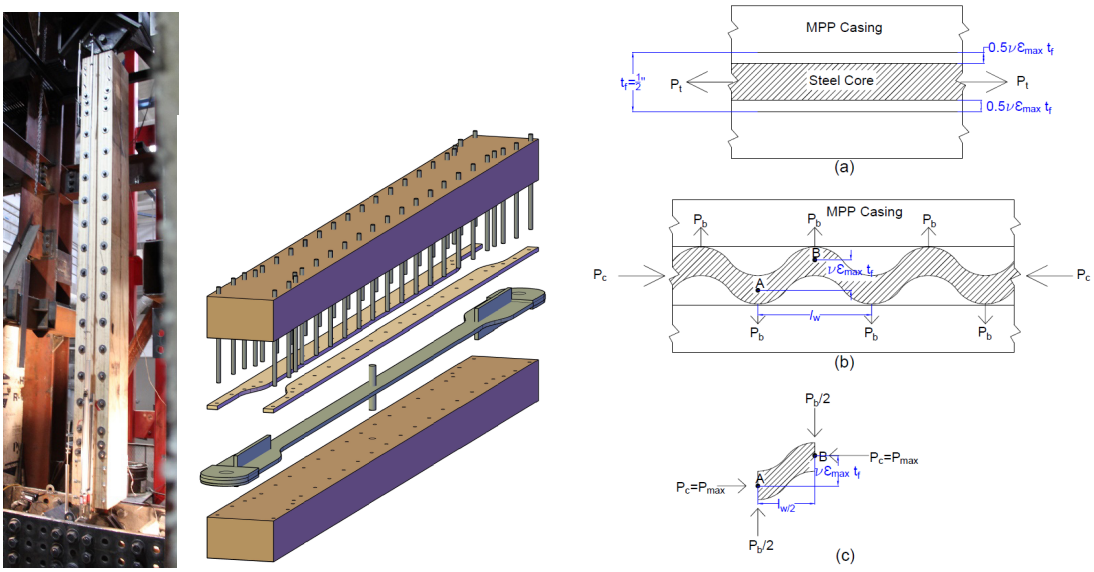

Fig. 5 – T-BRB design and internal mechanics of buckling: (a) tensile load; (b) compressive load; (c) free-body diagram

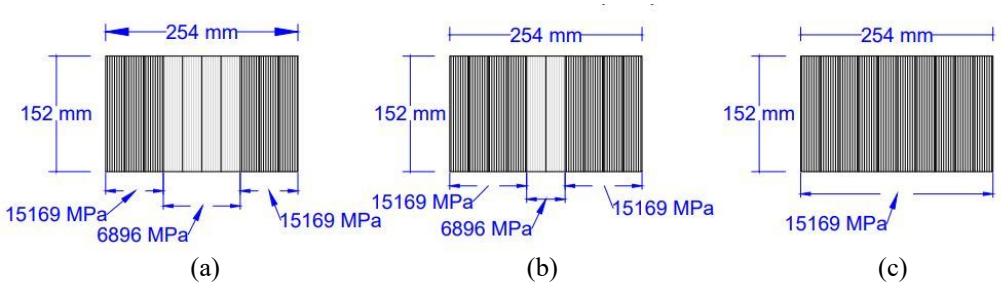

Fig. 6 – MPP layout detail for three specimen casing types: (a) soft; (b) medium; (c) hard

3.2 T-BRB loading program

Two loading protocols were used for the six T-BRB experiments: fatigue-based, as shown in Fig. 7(a) and high strain-based, as shown in Fig. 7(b). The fatigue-based cyclic loading protocol was developed using AISC-341-16 Chapter F4 and Appendix K3 [9]; cyclic drift was increased by 0.5% until a 2% drift ratio was reached; subsequently the drift ratio was reduced to 1.5%; finally, the 1.5% drift ratio was cycled until failure. In the high strain-based loading protocol, the T-BRB drift was increased by 0.5% until failure with the following steps: 0.5%, 1.0%, 1.5%, 2.0%, 2.5%, and 3.0%. The 2.49 m yield zone was used to calculate strain and axial displacement. AISC 341-16 qualification requires the brace to be tested to 2.0 times the design story drift and to achieve a Cumulative Inelastic Deformation (CID) of 200 times the yield deformation. To determine these protocols, the design story drift, Δ_{bm}, and the brace yield deformation, Δ_{by}, were determined. The value of Δ_{bm} was calculated as 1.00%, which is 32.5 mm. The brace yield deformation Δ_{by} was determined using structural mechanics as 4.0 mm. Cumulative inelastic deformation (CID) was calculated per AISC 341-16 table C-K3.1 [6]. CID is the accumulation of deformation, both positive and negative, beyond yield which is then converted to multiples of brace yield deformation, Δ_{by}. The adjustment factors were determined from actual data using the hysteresis curves shown in Fig. 8 for the fatigue load protocol and Fig. 9 for the high strain load protocol. The compressive adjustment factor β was calculated using the following equation:

$$1.00 < \beta = P_{max} / T_{max} < 1.50 \quad (3)$$

which is the ratio between the maximum measured compressive load and maximum measured tensile load per loading cycle; this must remain below 1.50 per AISC 341-16 [9]. The strain hardening adjustment factor was calculated using the following equation:

$$\omega = T_{max} / (R_y P_{ysc}) \geq 1.00 \quad (4)$$

where ω is the ratio between the maximum measured tensile load and the yield force per cycle. Since coupon tests were used to determine yield stress, R_y is equal to 1.0, and P_{ysc} is the axial yield strength of the steel core. The ω value should be greater than 1.0 according to AISC 341-16 [9].

3.3 T-BRB test results

Hysteresis curves for the three specimens tested using the fatigue load protocol are shown in Fig. 8 and for the three specimens tested using the high strain load are shown in Fig. 9. All hysteresis curves remained stable throughout each test. A summary of results from the six T-BRB tests is presented in Table 1. Specimen 1 failed in tension after 39 cycles as shown in Fig. 8(a); the steel core in this test fractured due to low cycle fatigue while the compressive adjustment factor, β, ranged from 1.05 to 1.20 and the strain hardening adjustment factor ω ranged from 1.00 to 1.40. Specimen 2 failed in compression after 35 cycles as shown in Fig. 8(b); the MPP layers ruptured from the compressive demand transferred from the steel core which buckled about the weak axis, as shown in Fig. 10(a); the compressive adjustment factor, β, ranged from 1.05 to 1.15 and the strain hardening adjustment factor ω ranged from 1.00 to 1.32. Specimen 3 failed in compression after 28 cycles, as shown in Fig. 8(c); this test failure was similar to specimen 2 because the MPP layers ruptured due to the load demand from weak axis buckling of the steel core shown in Fig. 10(b); the compressive adjustment factor, β, ranged from 1.03 to 1.20; the strain hardening adjustment factor ω ranged from 1.00 to 1.35.

Specimen 4 also failed in compression, but on the 13th cycle at 3.92% strain as shown in Fig. 9(a); weak axis buckling was the dominant failure mode as shown in Fig. 11(a) while the ultimate failure mode was a ruptured casing; the compressive adjustment factor, β, ranged from 1.04 to 1.23; the strain hardening adjustment factor ω ranged from 1.00 to 1.43. Specimen 5 failed in compression on the 12th cycle at 3.92% strain as shown in Fig. 9(b); both weak-axis and strong-axis buckling of the steel core were present but the failure mode was a ruptured and split casing; the compressive adjustment factor, β, ranged from 1.10 to 1.20; the strain hardening adjustment factor ω ranged from 1.00 to 1.38. Specimen 6 failed on the 13th cycle at 3.92% strain as shown in Fig. 9(c); strong-axis buckling of the steel core was dominant as shown in Fig. 11(b); the casing layers split and opened due to the strong axis buckling force; the compressive adjustment factor, β, ranged from 1.11 to 1.25; the strain hardening adjustment factor ω ranged from 1.00 to 1.41. The load transferred to the MPP from strong axis steel core buckling in specimens 4-6 worked to pull apart plywood laminations. This cross-lamination force exacerbated compression failures under high drift loading once laminations split apart. Figure 12 shows the split resulting from this type of failure mode.

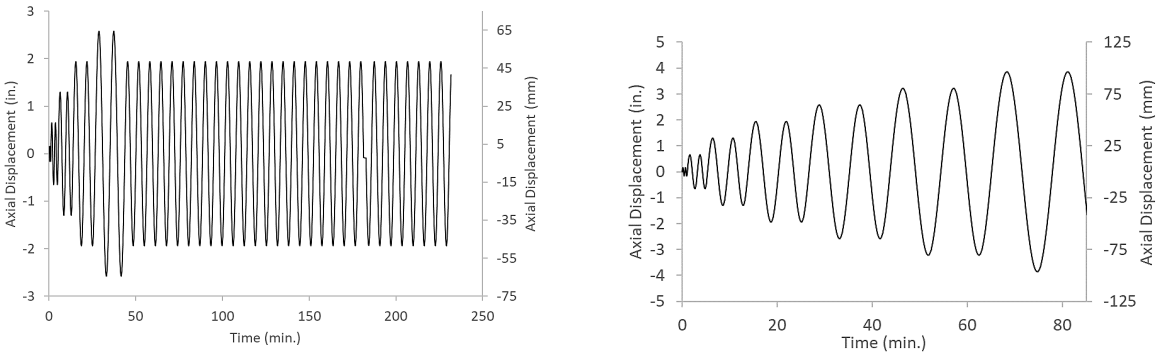

(a) (b)

Fig. 7 – Load protocols: (a) fatigue protocol for specimens 1-3; (b) high strain protocol for specimens 4-6

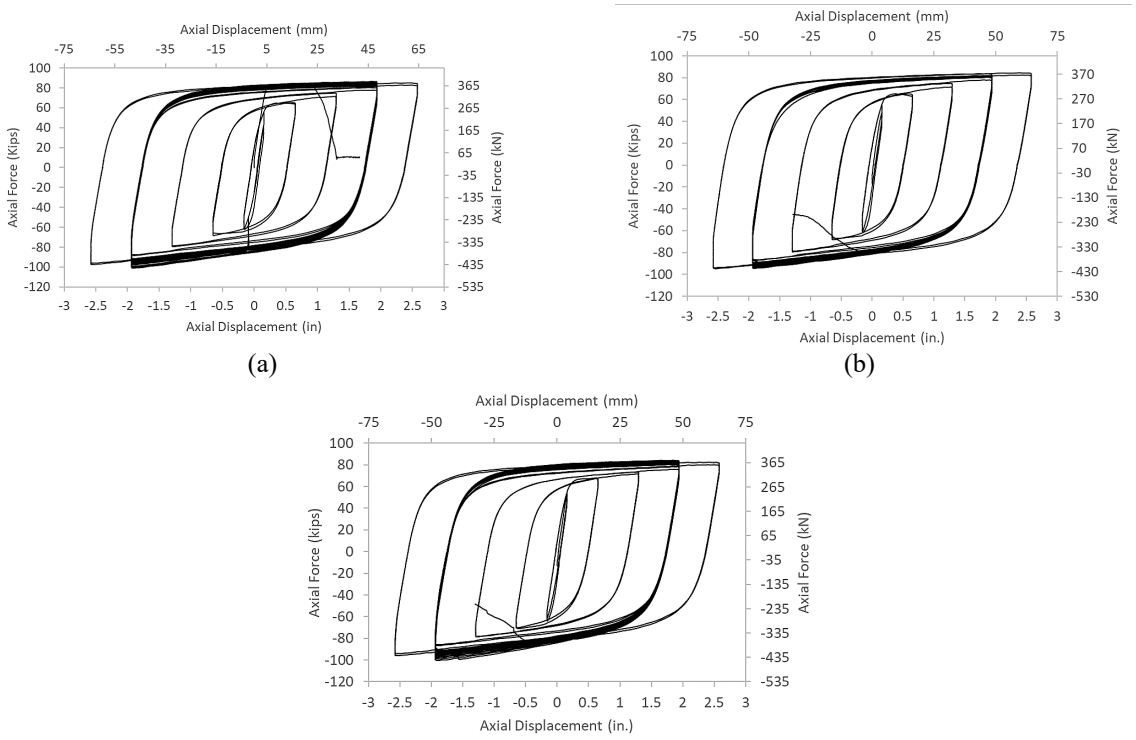

Fig. 8 – Hysteresis curves for fatigue load protocol: (a) specimen 1; (b) specimen 2; (c) specimen 3

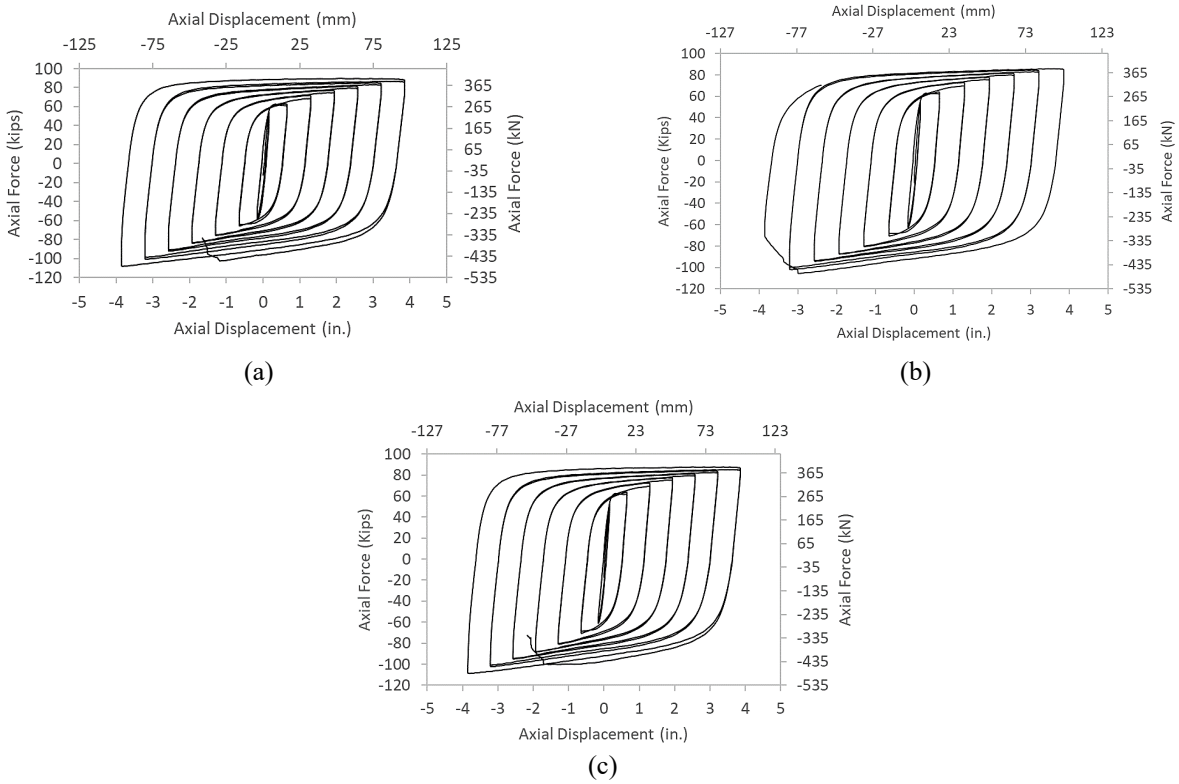

Fig. 9 – Hysteresis curves for high strain load protocol: (a) specimen 4; (b) specimen 5; (c) specimen 6

Table 1 – Results summary for T-BRB tests

Protocol Type	Specimen #	MPP Stiffness	Maximum Strain (%)	Cycles to Failure	CID	Hysteretic Energy (kN·m)
Fatigue	1	soft	2.61	39.0	1571	2194
	2	medium	2.61	35.5	1416	1902
	3	hard	2.61	28.5	1107	1487
Strain	4	hard	3.92	13.5	580	807
	5	medium	3.92	12.5	488	721
	6	soft	3.92	13.5	580	812

(a) (b)

Fig. 10 – Failure modes: (a) specimen 2; (b) specimen 3

(a) (b)

Fig. 11 – Failure modes: (a) specimen 4; (b) specimen 6

Fig. 12 – MPP split resulting from strong axis steel core buckling of specimen 6

4. Conclusions

Timber construction is establishing a reputation as sustainable and environmentally friendly. Timber is renewable with a good strength to weight ratio, good insulating properties and acts as a means to store carbon dioxide. Buckling-Restrained Braced Frames are a reliable method for providing an efficient lateral force resisting system in earthquake prone regions. The research presented shows that an efficient T-BRB is possible to construct and feasible to implement when combining a steel core with an engineered timber casing. The following conclusions can be drawn:

1. Unreinforced Glulam underperforms when compared to other engineered wood types; this wood type consistently fails before reaching 2.5 mm of displacement when loaded perpendicular to grain.

2. MPP loaded perpendicular to the wide face of the laminations without screw reinforcement also underperforms compared to MPP loaded parallel to the wide face of the laminations when considering elastic stiffness. The average elastic stiffness of samples loaded in the perpendicular orientation was 13.5 kN/mm while for samples loaded in the parallel orientation it was 45.0 kN/mm.

3. The T-BRBs tested in this research meet the requirements for uniaxial cyclic tests according to AISC 341-16. The hysteresis curves from these specimens prove that sufficient hysteretic energy dissipation is easily achievable and that stable damping performance is possible with a T-BRB.

4. Specimens 1-6 reached cumulative inelastic deformations of 1571, 1416, 1107, 580, 488, and 580 times the yield deformation, respectively, which outperforms the AISC 341-16 requirements that each tested brace must achieve a ductility corresponding to 2.0 times the design story drift and a cumulative inelastic axial ductility capacity of 200 times the yield deformation.

5. A 3.9% strain was sustainable for the three T-BRBs tested under the high strain loading protocol. The T-BRBs had a long fatigue life at 1.5% strain, after reaching a 2.6% strain, as shown for the three specimens tested under the fatigue loading protocol.

6. The compressive adjustment factor, β, remained below 1.50 thus satisfying AISC 341-16 for all six experiments; this factor ranged between 1.05 and 1.25. The strain hardening adjustment factor, ω, ranged from 1.00 to 1.41 thus satisfying AISC 341-16 for all six experiments.

7. The T-BRB developed in this research can be used in Buckling Restrained Braced Frames; it can be easily inspected after an earthquake to determine its condition and whether replacement of the steel core is necessary.

4. Acknowledgements

The authors would like to thank the U.S. Endowment for Forestry and Communities for the financial support. In addition, the authors want to thank the Forest Products Laboratory, Freres Lumber Co., Inc., and the Department of Civil and Environmental Engineering at the University of Utah and for their support and donation of time and materials. Additional thanks go to Vanessa McEntee, Mark Bryant, Bhaskar Kunwar, Duc Tran, Anurag Upadhyay, and Ryan Barton.

6. References

[1] Black CJ, Makris N, Aiken ID (2004): Component testing, seismic evaluation and characterization of buckling-restrained braces." *Journal of Structural Engineering*, **130** (6), 880–894.

[2] Blomgren H, Koppitz J, Valdes A, Ko E. (2016): The heavy timber buckling-restrained braced frame as a solution for commercial buildings in regions of high seismicity. *World Conference Timber Engineering*, Vienna, Austria.

[3] Popovski M (2000): Seismic performance of braced timber frames. Ph. D. thesis, Department of Civil Engineering, the University of British Columbia, Vancouver, B.C.

[4] Pryor SE, Flynn P, Downs W. (2014): Buckling restrained braced frame. (24-Nov-2005). Patent US 20050257490A1.

[5] Watanabe A, Hitomoi Y, Saeki E, Wada A, Fujimoto M (1988): Properties of brace encased in buckling-restraining concrete and steel tube. *Proceedings 9th World Conference on Earthquake Engineering*, Tokyo-Kyoto, Japan, 719-724.

[6] Wu A-C, Lin P-C, Tsai K-C (2013): "High-mode buckling responses of buckling-restrained brace core plates." *Earthquake Engineering & Structural Dynamics*, **43** (3), 375–393.

[7] Xu W, Pantelides CP (2017): Strong-axis and weak-axis buckling and local bulging of buckling-restrained braces with prismatic core plates. *Engineering Structures*, **153**, 279-289.

[8] Abrahamsen R (2017): Mjøstårnet-construction of an 81 m tall timber building. International Holzbau-Forum IHF.

[9] American Institute of Steel Construction (2016): Seismic provisions for Structural Steel Buildings, AISC 341, Chicago, Illinois.

